A liquid chromatography-mass spectrometry workflow for in-depth quantitation of fatty acid double bond location isomers

Jing Zhao[1], Mengxuan Fang[1,2], and Yu Xia[1]*

[1]MOE Key Laboratory of Bioorganic Phosphorus Chemistry & Chemical Biology, Department of Chemistry, Tsinghua University, Beijing, China; and [2]School of Chemistry, University of Melbourne, Melbourne, Victoria, Australia

Abstract Tracing compositional changes of fatty acids (FAs) is frequently used as a means of monitoring metabolic alterations in perturbed biological states. Given that more than half of FAs in the mammalian lipidome are unsaturated, quantitation of FAs at a carbon-carbon double bond (C=C) location level is necessary. The use of 2-acetylpiridine (2-acpy) as the charge-tagging PB reagent led to a limit of identification in the subnanomolar range for mono- and polyunsaturated as well as conjugated FAs. Conjugated free FAs of low abundance such as FA 18:2 (n-7, n-9) and FA 18:2 (n-6, n-8) were quantified at concentrations of 0.61 ± 0.05 and 0.05 ± 0.01 mg per 100 g in yak milk powder, respectively. This workflow also enabled deep profiling of eight saturated and 37 unsaturated total FAs across a span of four orders of magnitude in concentration, including ten groups of C=C location isomers in pooled human plasma. A pilot survey on total FAs in plasma from patients with type 2 diabetes revealed that the relative compositions of FA 16:1 (n-10) and FA 18:1 (n-10) were significantly elevated compared with that of normal controls. ⬛ In this work, we have developed a workflow for global quantitation of FAs, including C=C location isomers, *via* charge-tagging Paternò-Büchi (PB) derivatization and liquid chromatography-tandem mass spectrometry (LC-MS/MS).

Supplementary key words Fatty acids • double bond location isomers • quantitation • tandem mass spectrometry • liquid chromatography • lipidomics • type 2 diabetes • Paternò-Büchi • charge-tagging • 2-acetylpiridine

Fatty acids (FAs), existing either as free fatty acids (FFA) or building blocks of complex lipids, exert important functions such as energy source (1), membrane components (2), and precursors of signaling molecules in biological systems (3). The distribution of different molecular species of FAs in cell is tightly regulated to maintain normal cell function; dysregulation of FA homeostasis, such as an excessive degree of lipid saturation, impairs membrane integrity and causes lipotoxicity (4). In the *de novo* synthesis of unsaturated FAs, several desaturases and elongases work together and produce an array of C=C location isomers in mammalian lipidome (5). While knowledge on the exact functions of C=C location isomers is limited (6), increasing evidence suggests that alterations in the composition of C=C location isomers are highly sensitive to metabolic changes in cancer and other types of diseases (7, 8). Thus, profiling of FAs at C=C location level is desirable for both fundamental studies and biomedical applications where perturbed lipid metabolism is of research interest.

To date, gas chromatography hyphenated with electron ionization mass spectrometry (GC/EI-MS) is still widely used for profiling FAs, albeit in the form of fatty acid methyl esters (FAMEs) (9). Identification of FAs relies on matching the retention time of GC-separated FAMEs to those of the standards (10, 11), which inevitably limits its utility in the discovery of unknown FA species. FA derivatization *via* 4,4-dimethyloxazoline (DMOX) or pyrrolidides improves GC/EI-MS for the identification of C=C location; however, they have limitations for the analysis of polyunsaturated FAs (PUFAs) because not all C=C related fragments are generated (12, 13). Brenna and coworkers demonstrated coupling acetonitrile (ACN) chemical ionization (CI) with collision-induced dissociation (CID) for independent structural analysis of unsaturated FAMEs (14, 15). The development of electrospray ionization (ESI)-tandem mass spectrometry (MS/MS) has enabled large-scale profiling of FFAs and different classes of complex lipids either with or without hyphenation with liquid chromatography (16). However, the location of C=C in FAs is typically not obtained from these approaches. Alternative ion activation methods, which can provide detailed structural information, have been developed, including charge-remote fragmentation (17, 18), ozone-induced dissociation (OzID) (19), ultraviolet photodissociation (UVPD) (20, 21), ion/ion reactions (22), etc. On

the other hand, the combination of functional group-specific derivatization and MS^2 CID greatly expands the capability of detailed structural analysis of lipids on commercial MS platforms. Notable methods include epoxidation (23, 24), converting C=C to hydroperoxides *via* singlet oxygen (25), and the Paternò-Büchi (PB) reaction (26). The PB-MS/MS approach has been adopted by several groups and applied to common lipid analysis workflows, including shotgun (27), direct analysis (28), LC-MS (29), and MS imaging (30). Briefly, during the PB reaction, electronically excited carbonyl compound adds on to a C=C under UV/visible light irradiation (31), forming a four-membered oxetane ring at moderate yield. When subjected to ion activation (CID or UVPD (32)), the oxetane ring is preferentially dissociated, generating C=C diagnostic ions key to independent identification of C=C location and quantitation of C=C location isomers from mixtures (27). A schematic representation of the PB reaction and the diagnostic ions generated from subsequent PB-MS/MS is shown in **Fig. 1**A.

Acetone PB reaction was initially demonstrated for pinpointing C=C location in various monounsaturated FAs (MUFAs) and PUFAs from complex mixtures (33, 34). This method, however, showed relatively low sensitivity due to the need to perform MS^2 CID of the lithium adduct ions of the PB products in positive ion
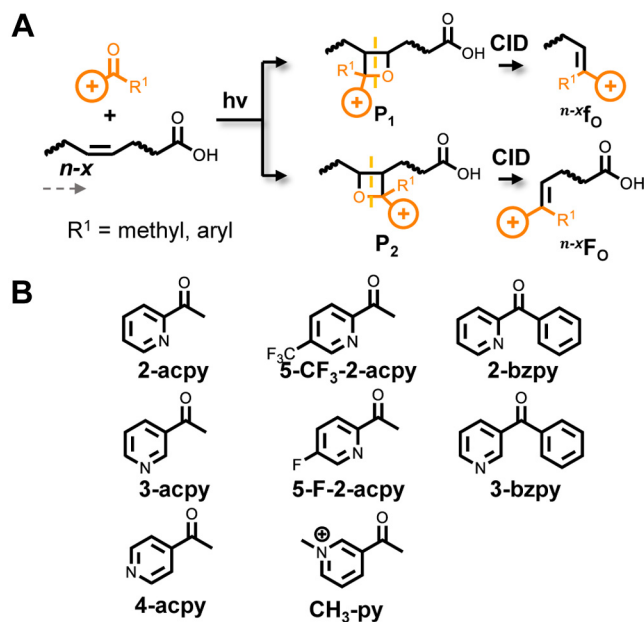
mode. Xu *et al.* (35) recently showed a two-step derivatization strategy to enhance the analysis of FAs, in which the acetone PB reaction was followed by derivatizing the carboxylic group with N, N-diethyl-1,2-ethanediamine. Alternatively, Heiles and coworkers showed that the PB derivatization and charge-tagging could be achieved in one step by using a PB reagent containing a functional group readily to be protonated via ESI, such as 3-acetylpyridine (3-acpy) (36). Our group recently demonstrated 2-acetylpyrindine (2-acpy) as a highly efficient charge-tagging PB reagent for the analysis of cholesterol esters (CEs) at sub-nM range of limit of identification (LOI) (37).

The above findings motivated us to develop a sensitive and readily adaptable workflow for quantitation of FAs at C=C location level *via* charge-tagging PB derivatization. From eight PB reagents being screened, 2-acpy was chosen as the best reagent considering its commercial availability, relatively high signal enhancement, and low LOI (0.5 nM for FA standards). An LC-MS workflow was thus established for in-depth quantitation of both saturated and unsaturated FAs. It consisted of two offline derivatization steps, namely N-[4-(aminomethyl)phenyl]pyridinium (AMPP) derivatization for quantitation of FAs at fatty acyl chain level (17) and 2-acpy derivatization for quantitation of unsaturated FAs at C=C location level. The above workflow enabled quantitation of several low-abundance C=C location isomers, such as conjugated FA 18:2 (n-7, n-9) in yak milk powder and FA 16:1 (n-10) in pooled human plasma. This workflow was further applied for monitoring the change of FA profiles in plasma samples from type 2 diabetes (T2D) patients relative to normal control.

Fig. 1. A: Schematic presentation of the charge-tagging PB reaction and C=C diagnostic ions formed from PB-MS^2 CID. Different orientations of the PB reagent relative to the C=C produce two types of PB products, P_1 and P_2. For PB-MS^2 CID only C=C diagnostic ions are shown, one containing methyl end ($^{n-x}f_O$) while the other containing carboxylic group ($^{n-x}F_O$). Superscript *n-x* denotes the location of C=C counting from the methyl terminus. Subscript "O" defines that the fragment contains olefin functional group at the cleavage site. B: A list of acetylpyridine derivatives tested as the charge-tagging PB reagents for FA analysis.

MATERIALS AND METHODS

Lipid nomenclature

To facilitate tracing unsaturated FAs derived from the same desaturation process but different elongation steps in biological samples, the position of C=C in an aliphatic chain is defined by the *n-x* nomenclature, counting from the methyl terminus. For example, FA 18:2 (n-6, n-9) denotes a fatty acid containing 18 carbons with two C=C bonds at sixth and seventh and ninth and tenth carbons from the methyl terminus of the acyl chain. The Z/E stereo-configurations of C=C could not be assigned from PB-MS/MS and thus were not indicated for FAs from biological samples.

Materials and chemicals

All organic solvents and reagents were purchased commercially and used without further purification. FA standards and AMP$^+$ MaxSpec Kit were purchased from Cayman Chemical (Ann Arbor, MI). Charge-tagging PB reagents, including 2-, 3-, and 4-acpy, 1-(5-(fluoro)pyridin-2-yl) ethanone (5-F-2-acpy), 1-(5-(trifluoromethyl)pyridin-2-yl)ethanone (5-CF$_3$-2-acpy), and 2-benzoylpyridine (bzpy) were purchased from Bidepharm (Shanghai, China). 3-Acetyl-1-

methylpyridinium (CH3-py) was purchased from Sigma-Aldrich (St. Louis, MO). Pooled normal human plasma with anticoagulant lithium heparin added was obtained from Innovative Research, Inc. (Novi, MI). Plasma samples from T2D patients and normal control were supplied by the specimen bank of Dongfeng Hospital of Hubei University of Medicine. The human studies abided by the Declaration of Helsinki principles. All the procedures related to these samples were compliant with relevant ethical regulations approved by the Ethical Review Board of Tsinghua University (IRB No. 2017007). Yak milk powder was purchased from market (Liaoyuan Dairy LTD, Gansu, China). HPLC grade ACN, methanol (MeOH), and isopropanol (IPA) were purchased from Fisher Scientific Company (Ottawa, ON, Canada).

Lipid extraction and sample preparation

Total lipids were extracted from 50 µl human plasma with [D4] FA 18:0 (25 nmol) added as internal standard (IS) according to a modified Folch method (29). The plasma sample was placed in a 10 ml-centrifuge tube containing 1 ml water, 1 ml MeOH, and 2 ml chloroform. The sample was vortexed for 5 min and centrifuged at 12,000 rpm for 10 min. The bottom layer was collected. The same amount of chloroform was added and the extraction process was repeated once. The chloroform layers were combined and dried under nitrogen flow. The extracted lipids were then saponified in 500 µl MeOH:15% KOH (50/50, v/v) at 37 °C for 30 min. The solution was acidified with 1 M HCl (1 ml). The hydrolyzed lipids were extracted twice with 1.5 ml isooctane each time. The organic layer was collected, dried under nitrogen, and redissolved in an aliquot of 500 µl MeOH for further derivatization. FFAs in 100 mg yak milk powder (with 25 nmol IS added) were extracted using H2O/MeOH/isooctane procedure (9, 34). Briefly, the milk sample was dissolved in a solution containing 1.25 ml Dulbecco's phosphate-buffered saline (dPBS), 1.5 ml MeOH, and 50 µl 1 M HCl. After an addition of 2.5 ml isooctane, the sample was vortexed for 5 min and centrifuged at 12,000 rpm for 10 min. After collecting the upper layer, the extraction process was repeated once. The organic layers were combined, dried under nitrogen gas, and redissolved in 500 µl MeOH. FFAs in 100 µl human plasma (with 0.5 nmol IS added) were processed following the same procedure and redissolved in 100 µl MeOH.

AMPP derivatization

AMPP derivatization followed the procedure provided by the vendor (AMP+ MaxSpec Kit). Lipid extracts (25 µl MeOH solution) were dried by nitrogen flow, then dissolved in a solution containing 10 µl 4:1 ACN/DMF, 10 µl 1-ethyl-3-(3-dimethylaminopropyl) carbodiimide (EDC) (640 mM in H2O), 5 µl N-hydroxybenzotriazole (HOBt) (20 mM in 99:1 ACN/DMF), and 15 µl AMPP (20 mM in ACN), and incubated at 60 °C for 30 min. After cooling to room temperature, the solution was added with 600 µl water. AMPP derivatized sample was extracted twice by 600 µl methyl tert-butyl ether (MTBE) and dried under nitrogen stream. The derivatized sample was resuspended in 125 µl MeOH for LC-MS/MS analysis. Because FA 16:0 and FA 18:0 are ubiquitously present in the background, relative quantitation of FA 16:0 and 18:0 in blank samples was performed, and then they were subtracted for relative quantitation of these two FAs in biological samples (supplemental Fig. S1).

Offline PB derivatization

The PB derivatization was performed using a home-made flow microreactor (38). FA standards (5 µM each) or FA extracts dried from 50 µl solution and 10 mM PB reagent were dissolved in 100 µl ACN. The solution was injected into the flow microreactor for 10–25 s UV irradiation (~254 nm). About 50 µl reaction solution was collected; the excess reagent was washed by 600 µl HCl solution (10 mM). The PB derivatized sample was extracted twice by 600 µl isooctane and dried under nitrogen flow. The PB derivatized sample was resuspended in 50 µl MeOH before subsequent RPLC-MS/MS analyses. Because the synthetic standards for most of C=C location isomers detected from biological samples were not available, relative quantitation of isomer composition was performed. First, the peak intensities of the C=C diagnostic ions, namely $^{n-x}F_O$ and $^{n-x}f_O$, were summed as $\sum I_{n-x}$. Then, the relative composition of the n-x C=C isomer was calculated as $\sum I_{n-x} / (\sum I_{n-x} + \sum I_{n-y} + \sum I_{n-z}\ldots)$, in which n-y and n-z represented other detected C=C location isomers from the same PB-MS^2 CID spectrum. For FA 18:2 in yak milk powder, the synthetic standards of the isomers were available; therefore, each isomer was quantified from the calibration curves.

LC-MS/MS analyses

Reversed-phase (RP) LC-MS/MS analyses were conducted on a Shimadzu LC-20AD system (Kyoto, Japan) hyphenated with an X500R QTOF mass spectrometer (Sciex, Toronto, Canada). The injection volume was 2 µl per run. A C18 column (150 mm × 3.0 mm, 2.7 µm, Sigma-Aldrich, MO) was used for separation. The mobile phase A contained H2O:ACN (40:60, v/v, added with 20 mM ammonium formate) and mobile phase B contained IPA:ACN (40:60, v/v, added with 0.2% HCOOH). The flow rate was set at 0.45 ml/min. The chromatographic gradient was as follows: 30% B at 0–0.75 min, 30%–45% B at 0.75–2 min, 45%–52% B at 2–2.5 min, 52%–58% B at 2.5–4 min, 58%–66% B at 4–5.5 min, 66%–70% B at 5.5–7 min, 70%–75% B at 7–9 min, 75%–97% B at 9–10 min, 97% B at 10–13 min, 30% B at 13.1–15 min. The MS parameters were optimized as follows: ESI voltage, 4500 V; curtain gas, 35 psi; interface heater temperature, 450 °C; nebulizing gas 1 and gas 2, 30 psi; declustering potential, 100 V, CID energy for MS/MS, 18–25 eV; and CID energy for MRM, 50 eV.

RESULTS

Screening charge-tagging PB reagents

A series of carbonyl compounds containing pyridine ring were tested as charge-tagging PB reagents (structures listed in Fig. 1B). FA 18:1(n-9Z) was used as a model compound (5 µM in ACN) while the concentration of each PB reagent was kept in large excess (10 mM in ACN). We found that 15 s UV irradiation was adequate to drive the reaction to a steady state. The reaction solution was then subjected to LC-MS/MS for product analysis. **Figure 2**A represents a typical extracted ion chromatogram (EIC) of the reaction products due to one PB reagent addition to FA 18:1(n-9Z) using 2-acpy as an example ([FA+2-acpy+H]+, m/z 404.3). Besides the major components (76% of total peak area) eluted around 6.3 min, there are several smaller peaks, suggesting the presence of side reaction products. In the MS^2 CID spectrum of the major peaks (Fig. 2B), the
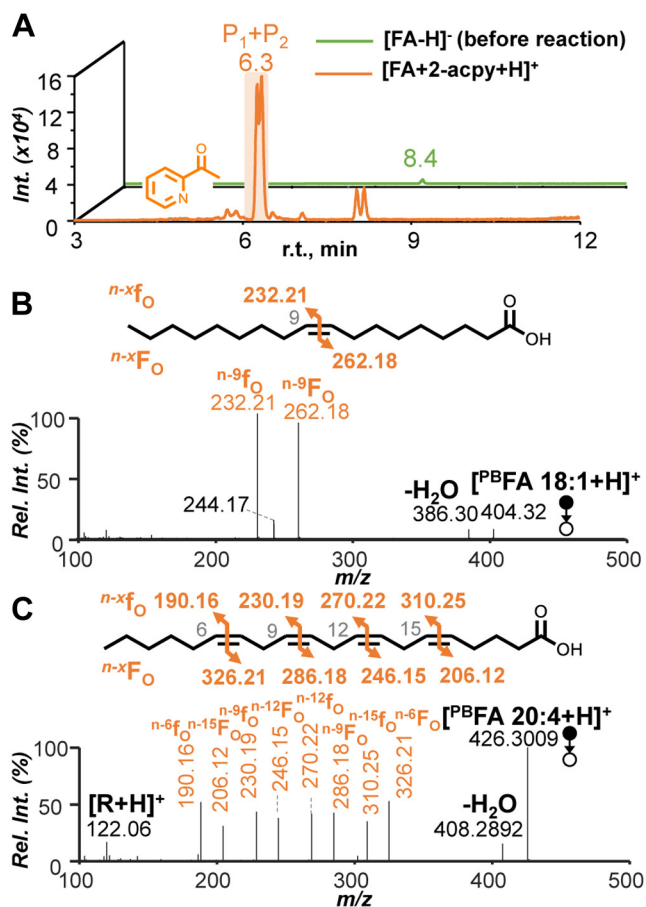
Fig. 2. A: EICs of 5 μM intact FA 18:1(n-9Z) ([FA-H]⁻, *m/z* 281.3, green trace) and 2-acpy modified FA ([FA+2-acpy+H]⁺, *m/z* 404.3, orange trace). B: PB-MS² CID of FA 18:1(n-9Z) (*m/z* 404.3 eluted from 6.2 min to 6.4 min). C: PB-MS² CID of the PB product from 2-acpy and FA 20:4(n-6Z, n-9Z, n-12Z, n-15Z) (*m/z* 426.3 eluted from 4.9 min to 6.0 min).

expected C=C diagnostic ions are present, *i.e.*, $^{n-9}f_O$ (*m/z* 232.21) and $^{n-9}F_O$ (*m/z* 262.18), proving that they are derived from the PB products, P_1 and P_2 (generic structures shown in Fig. 1A). MS² CID of the peaks eluted before the PB products (3.0–6.0 min) produced a dominant water loss peak (*m/z* 386.3), while MS² CID of the peaks eluted later than the PB products (8.0–8.3 min) only produced a fragment peak corresponding to the protonated PB reagent (*m/z* 122.1). These side reaction products are likely formed from the competing Norrish Type II reactions, and they share the same mass as the PB products (9, 38). The CID spectra and possible structures of these side reaction products are provided in supplemental Fig. S2.

The performance of each reagent for the analysis of unsaturated FA was evaluated based on two criteria: the enhancement of ion signal of the derivatized FA relative to intact FA in MS¹ and the capability in generating abundant C=C diagnostic ions from PB-MS² CID. Enhancement factor *x* was calculated by dividing the EIC peak area of the PB products in positive mode (*e.g.*,

for 2-acpy, the peaks eluted from 6.1 to 6.3 min, orange trace in Fig. 2A) by that of the intact FA in negative ion mode (the peak eluted around 8.4 min, green trace, Fig. 2A). Among all tested reagents, 5-CF₃-2-acpy, 3-acpy, 2-acpy, and 3-bzpy showed much higher signal enhancement than the rest, with *x* around 90 and moderate extent of Norrish Type II side reactions (10%–30%) (supplemental Table S1). Regarding forming C=C diagnostic ions, only $^{n-x}f_O$ type of diagnostic ions were generated from 3-acpy and 3-bzpy from PB-MS² CID, while both $^{n-x}f_O$ and $^{n-x}F_O$ ions were produced from 5-CF₃-2-acpy and 2-acpy (supplemental Fig. S3). The absence of $^{n-x}F_O$ was found unfavorable for unambiguous identification of conjugated FAs as discussed in the later section. Considering that 2-acpy is more economic than 5-CF₃-2-acpy, which was custommade, 2-acpy was chosen as the charge-tagging PB reagent for further development of the FA analysis workflow.

Under the optimized reaction condition, *i.e.*, 10 mM 2-acpy and 15 s of irradiation, the LOI for FA 18:1(n-9Z) was achieved at 0.5 nM (0.3 pg for each injection) from LC-MS/MS based on detecting the diagnostic ions three times above the noise level (supplemental Figs. S4 and S5). As to the analysis of PUFA, MS² CID of [^{PB}FA 20:4+H]⁺ (*m/z* 426.3) produced four pairs of C=C diagnostic ions, allowing pinpointing C=C at n-6, 9, 12, and 15, respectively (Fig. 2C). The yield of PB reaction at different double bond position in FA 20:4 was similar based on the EIC peak area of individual PB products (supplemental Fig. S6). Consistent to our previous findings, the yield of the 2-acpy PB reaction of 18:1(n-9E) as well as the PB-MS² CID spectrum was almost identical to those of FA 18:1(n-9Z) (supplemental Fig. S7). Thus, PB-MS/MS cannot distinguish the cisversus trans-configuration of a C=C due to fast photoisomerization of the C=C during the reaction (39). We also explored MS² CID of the charged PB products in negative ion mode, *i.e.*, [FA+2-acpy-H]⁻; however, neutral loss of reagent was the dominant fragment peak with little C=C diagnostic ions being formed (supplemental Fig. S8). When a fixed-charge PB reagent such as CH₃-py was used, no C=C diagnostic ions were observed in the MS² CID spectrum under positive mode (supplemental Fig. S8). The above findings suggest that mobile proton is likely key to facilitate the cleavage of oxetane ring and form C=C diagnostic ions.

RPLC-MS/MS workflow for relative quantitation of FAs at C=C location level

Nine FA standards varying in chain lengths (C14-24) and degrees of unsaturation (1–6) were subjected to 2-acpy derivatization and subsequent RPLC-MS/MS analysis. The retention time of 2-acpy tagged FAs increased linearly with chain length for a given degree of unsaturation (supplemental Fig. S9). Interestingly, 2-acpy derivatization of FAs provided improved

separation of C=C location isomers *via* RPLC. As shown in **Fig. 3**A, B the EICs of $^{n\text{-}x}f_O$ ions derived from PB-MS^2 CID of FA 16:1(n-7Z), FA 16:1(n-9Z), and FA 16:1(n-10Z) are almost baseline-separated. Small shoulder peaks in Fig. 3B correspond to unresolved stereoisomers of the PB products. As a comparison, only partial separation of the C=C location isomers of the intact FAs ([FA-H]$^-$, *m/z* 253.2) was achieved (Fig. 3C). The order of elution of these isomers stayed unchanged before or after derivatization, with the isomers containing C=C closer to the methyl terminus eluted earlier. This feature was found useful in confirming the assignment of low abundance isomers in mixture analysis.

The procedure for relative quantitation of C=C location isomers was established using a set of solutions containing FA 16:1(n-7Z) and FA 16:1(n-9Z) with molar ratios ranging from 1:1 to 29:1 while the total concentration was kept at 5 μM. Such a molar ratio range is based on the natural distribution in mammalian cells, where FA 16:1(n-7Z) is the major isomer resulting from Δ9 desaturation of palmitic acid by stearoyl-CoA desaturase (SCDs) (5).The summed ion abundances of the $^{n\text{-}x}F_O$ and $^{n\text{-}x}f_O$ from each isomer were calculated and the ratios of that from n-7 over n-9 were plotted against the molar ratios of the two isomers. Good linear relationship ($R^2 = 0.9938$) was
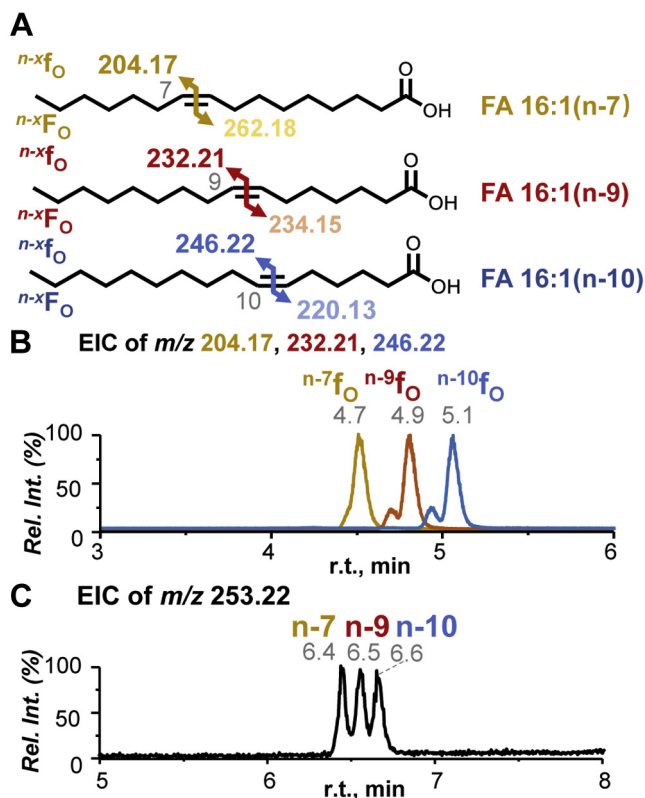
achieved with a slope close to unity (0.9827) (black dotted line in **Fig. 4**A). FA 16:1(n-10Z) is the desaturation product of palmitic acid by FADS2 and its level reflects FADS2 activity (8, 40). We thus developed a relative quantitation procedure for FA 16:1(n-10Z) using a set of solutions containing FA 16:1(n-9Z) and FA 16:1(n-10Z). Good linearity ($R^2 = 0.994$, slope = 0.9083) in a wide dynamic range was also obtained for the calibration curve (green dotted line in Fig. 4A). These data suggest that a quick estimation of the composition of C=C location isomers can be inferred from the relative ion abundances of the C=C diagnostic ions for the three isomers of FA 16:1.

Conjugated linoleic acids (CLA) are another major type of C=C isomers of linoleic acid (LA or FA 18:2(n-6Z, n-9Z)) found in dairy product (41). In ruminant fat, FA 18:2(n-7E, n-9Z) occupies about 90% of total CLA, followed by FA 18:2(n-6Z, n-8E) (42). The PB reactions between 2-acpy with conjugated C=C demonstrated regioselectivity, consistent to that observed from acetone PB reactions (43). The PB products of FA 18:2(n-7E, n-9Z) consisted dominantly of P_1 at n-9 and P_2 at n-7; thus PB-MS^2 CID generated only $^{n\text{-}9}f_O$ (*m/z* 230.19) and $^{n\text{-}7}F_O$ (*m/z* 288.20) (Fig. 4B, C). Similarly, PB-MS^2 CID of FA 18:2(n-6Z, n-8E) produced $^{n\text{-}8}f_O$ (*m/z* 216.17) and $^{n\text{-}6}F_O$ (*m/z* 302.21). As a comparison, PB-MS^2 CID of FA 18:2(n-6Z, n-9Z) produced two pairs of diagnostic ions $^{n\text{-}6}f_O$, $^{n\text{-}6}F_O$ (*m/z* 190.16, 302.21) and $^{n\text{-}9}f_O$, $^{n\text{-}9}F_O$ (*m/z* 230.19, 262.18) (Fig. 4D). Therefore, distinct fragment ions of each isomer, i.e., $^{n\text{-}7}F_O$ (*m/z* 288.20) of FA 18:2(n-7, n-9), $^{n\text{-}8}f_O$ (*m/z* 216.17) of FA18:2(n-6, n-8), and $^{n\text{-}6}f_O$ (*m/z* 190.16) of FA 18:2(n-6, n-9) can be selected for identification and quantitation. Indeed, calibration curves were obtained with good linearity for FA 18:2(n-7, n-9)/FA 18:2(n-6, n-8) ($R^2 = 0.9987$) and FA 18:2(n-6, n-9)/ FA 18:2(n-7, n-9) ($R^2 = 0.9997$), respectively (Fig. 4E). Because the yield of PB reaction for CLA was lower than that of LA (supplemental Fig. S10), the slope of the calibration curve of FA 18:2(n-6, n-9)/ FA 18:2(n-7, n-9) deviated from unity.

The yield of the PB reaction may vary from batch to batch, and it is also affected by the chemical nature of a C=C, such as conjugated versus isolated C=C; however, these factors have no obvious effect on the quantitation of isomer composition (27). We compared I($^{n\text{-}7}F_O$ + $^{n\text{-}7}f_O$) / I($^{n\text{-}9}F_O$ + $^{n\text{-}9}f_O$) from an equal molar mixture of the n-7 and n-9 isomers of FA 16:1 at four different reaction time points: 5 s, 10 s, 15 s, and 20 s. Although the reaction yields were quite different, the peak intensity ratio showed little variation, with an average value of 0.94±0.01 from four reaction time points (supplemental Fig. S11). The same phenomenon was observed for the mixture of FA 18:2(n-6Z, n-9Z) and FA 18:2(n-7E, n-9Z), in which the PB conversion of the isolated C=Cs was about twice of that of the conjugated C=Cs (supplemental Fig. S12).

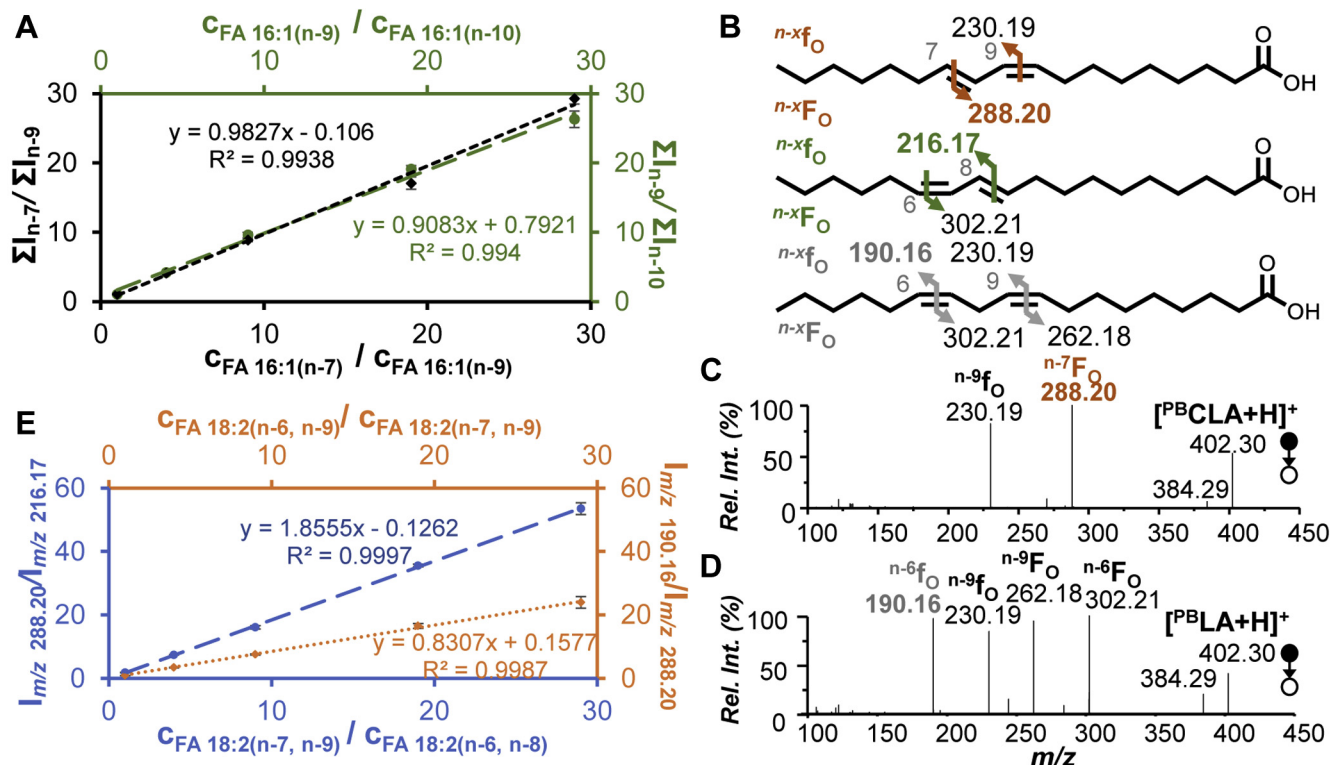The above relative quantitation methods allow obtaining molar ratio composition of C=C location

Fig. 3. A: Fragmentation schemes of FA 16:1 C=C location isomers (synthetic standards): n-7Z, n-9Z, and n-10Z; (B) EICs of the diagnostic ions: $^{n\text{-}7}f_O$ in yellow trace, $^{n\text{-}9}f_O$ in red trace, and $^{n\text{-}10}f_O$ in blue trace. C: EICs of intact C=C location isomers ([FA 16:1-H]$^-$ at *m/z* 253.2).

Fig. 4. A: Ratio plots of ion abundances of the diagnostic ions against molar ratios of corresponding C=C location isomers of FA 16:1: n-7/n-9 in black and n-9/n-10 in green. B: Fragmentation schemes of FA 18:2(n-7E, n-9Z), FA 18:2(n-6Z, n-8E), and FA 18:2(n-6Z, n-9Z); (C) PB-MS² CID of CLA: FA 18:2(n-7E, n-9Z); (D) PB-MS² CID of LA: FA 18:2(n-6Z, n-9Z); (E) ratio plots of ion abundances of the unique C=C diagnostic ions against molar ratios of the corresponding isomers of FA 18:2: FA 18:2(n-6, n-9)/FA 18:2(n-7, n-9) in orange and FA 18:2(n-7, n-9)/FA 18:2(n-6, n-8) in blue. Error bars represent the standard deviation of the mean (N = 3).

isomers. To achieve concentration information of each isomer, it is necessary to acquire total concentration of the isomers. We thus performed AMPP derivatization and used MRM transition from $[^{AMPP}FA]^+$ to m/z 183.1, a characteristic AMPP fragment peak, to quantify both saturated and unsaturated FAs at chain composition level (17, 44). The calibration curves of FA 16:1 (n-7Z), FA 18:1 (n-10Z), FA 18:2 (n-6Z, n-9Z), and FA 20:4 (n-6Z, n-9Z, n-12Z, n-15Z) are provided in supplemental Fig. S13 using [D4] FA 18:0 as the IS. Good linear relationship was obtained in a wide linear dynamic range for different number of carbons, degree of unsaturation, and C=C positions, consistent to a previous report by Han and coworkers (17). When authentic standards can be obtained, the concentration of each C=C isomer can be determined by combining the two-step relative quantitation procedure, while quantitation of saturated FAs can be directly achieved from MRM of $[^{AMPP}FA]^+$. Han and coauthors have demonstrated relative quantitation of FA C=C location isomers *via* multiple linear regression analysis of all fragment ions generated from MS² CID of AMPP derivatized FAs (17). As a comparison, PB-MS/MS method provides a simpler means for relative quantitation of isomers, especially when the synthetic standards are not available for performing multiple linear regression analysis.

Profiling FFAs at C=C location level in yak milk powder

Dairy products are important component of the Western diet, and they contain diverse distribution of FAs, which are frequent subjects of study for health effects (45). We applied the developed workflow for the analysis of FFA in yak milk powder. A total of 33 FFAs were profiled at sum composition level; they consisted of medium-chain (carbon number: 7–12), long-chain (carbon number: 13–21), and very-long-chain FAs (carbon number >21) with up to 6 C=C bonds (Fig. 5A). FA 18:1, FA 16:0, FA 18:0, FA 18:2, and FA 14:0 were detected as the more abundant FFAs, while unsaturated FFAs of odd-carbon number chain, such as FA 15:1, FA 17:1, and FA 19:1, were detected at 2–3 orders of magnitude lower relative abundances than that of FA 16:0. The corresponding data set is provided in supplemental Table S2, including retention time and the m/z of precursor ions in MRM transitions. Biosynthesis in rumen microbiome is believed as the source of FAs of odd-carbon number chain as well as conjugated C=C bonds (41). From PB-MS/MS analysis, FA 15:1 was identified as FA 15:1(n-6) (supplemental Table S3). For FA 17:1 and FA 19:1, the n-8 (81%) and n-10 (84%) isomers were the major components, respectively (Fig. 5B). FA 18:2(n-6, n-9) was identified as the dominating isomer of FA 18:2; however, two conjugated isomers, FA 18:2(n-7, n-9) (27%) and FA
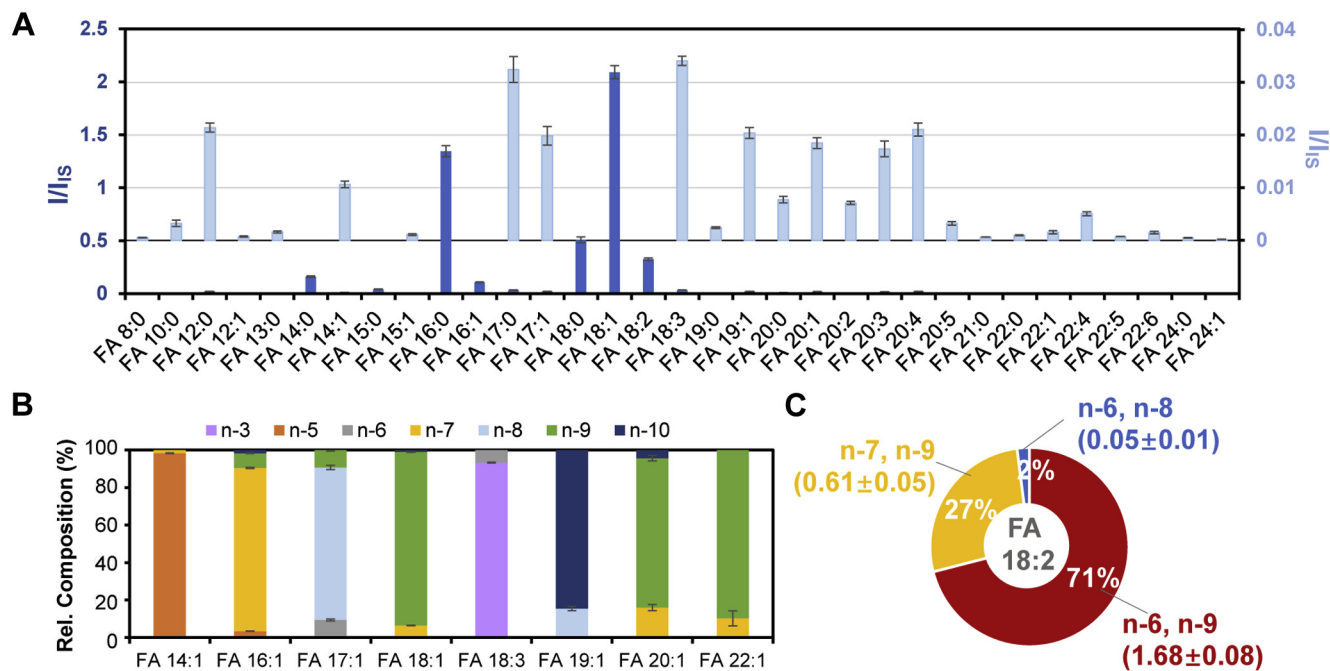
Fig. 5. A: Relative quantitation of FFAs at sum composition level in yak milk powder. B: Relative compositions (%) of C=C location isomers in eight groups of FAs. Error bars represent standard deviation of the mean (N = 3). C: Quantitation of three C=C location isomers of FA 18:2 in yak milk powder. Numbers in parenthesis represent the concentration of each isomer in units of mg per 100 g yak milk powder.

18:2(n-6, n-8) (2%), were also detected (Fig. 5C, PB-MS[2] CID spectrum shown in supplemental Fig. S14). The concentrations of FA 18:2(n-6, n-9), FA 18:2(n-7, n-9), and FA 18:2(n-6, n-8) were quantified to be 1.68 ± 0.08, 0.61 ± 0.05, and 0.05 ± 0.01 mg per 100 g yak milk powder, respectively. In total, 32 unsaturated FAs with C=C position information and 14 saturated FAs were detected in yak milk powder. Compared with the identified species by GC-MS analysis (46), nearly twice as many unsaturated FAs with detailed C=C location information were identified in this work. The increased annotation capability is attributed to the sensitive and independent identification of minor C=C location isomers *via* PB-MS/MS.

Profiling FAs at C=C location level in human plasma

The above workflow was applied for the analysis of total FAs in pooled human plasma. Relative quantitation of eight saturated FAs and eighteen unsaturated FAs was achieved at sum composition level based on MRM of AMPP derivatized FAs (**Fig. 6**A). The corresponding data set is provided in supplemental Table S4, including retention time and the *m/z* of precursor ions in MRM transitions. FA 18:1, FA 18:0, and FA 18:2 were the most abundant FA, MUFA, and PUFA, respectively. Offline derivatization by 2-acpy and subsequent RPLC-MS[2] CID led to the determination of 37 unsaturated FAs with confident assignment on C=C location. A full list of the identified FAs is documented in the supplemental Table S5. Among

these, ten groups of C=C location isomers were identified and quantified for relative composition, including FA 14:1, FA 16:1, FA 18:1, FA 18:3, FA 20:1, FA 22:1, FA 22:5, and FA 24:5 (Fig. 6B). The major C=C location isomers in the MUFAs are either directly or indirectly generated from the SCD family (Δ^9 desaturase). For instance, FA 16:1(n-7) and FA 18:1(n-9) can be *de novo* synthesized from palmitic acid and stearic acid by the SCD (Δ^9 desaturase) in mammalian cell, respectively (5). FA 16:1(n-7) is the precursor of the n-7 isomer family, *i.e.*, FA 18:1(n-7) and FA 20:1(n-7), while FA 18:1(n-9) is the precursor of other n-9 isomers containing 20–24 carbons in mammalian cells (5). The nonconical process of SCD can also produce FA 14:1(n-5), elongation of which forms FA 16:1(n-5). FA 16:1(n-9) was recently discovered to be formed *via* β-oxidation of FA 18:1(n-9) in monocytes (47). FA 16:1(n-10) should result from desaturation of FA 16:0 by FADS2(Δ^6 desaturase) (48); its elongation product is FA 18:1(n-10) (47). The relative composition of isomers should provide insights into the activation or deactivation of corresponding pathways.

Because of the lack of synthetic standards for several C=C location isomers detected in human plasma, only relative composition is reported here. Four C=C location isomers of FA 16:1 were analyzed for their relative compositions (Fig. 6C and supplemental Fig. S15). The most abundant isomer was FA 16:1(n-7), accounting for 83.9 ± 0.6%, followed by n-9 isomer (9.9 ± 0.1%), n-5 (3.7 ± 0.1%), and n-10 (2.4 ± 0.6%). For FA 18:1, FA 18:1(n-9) dominated (89.4 ± 0.1%), while the n-7 and the n-10
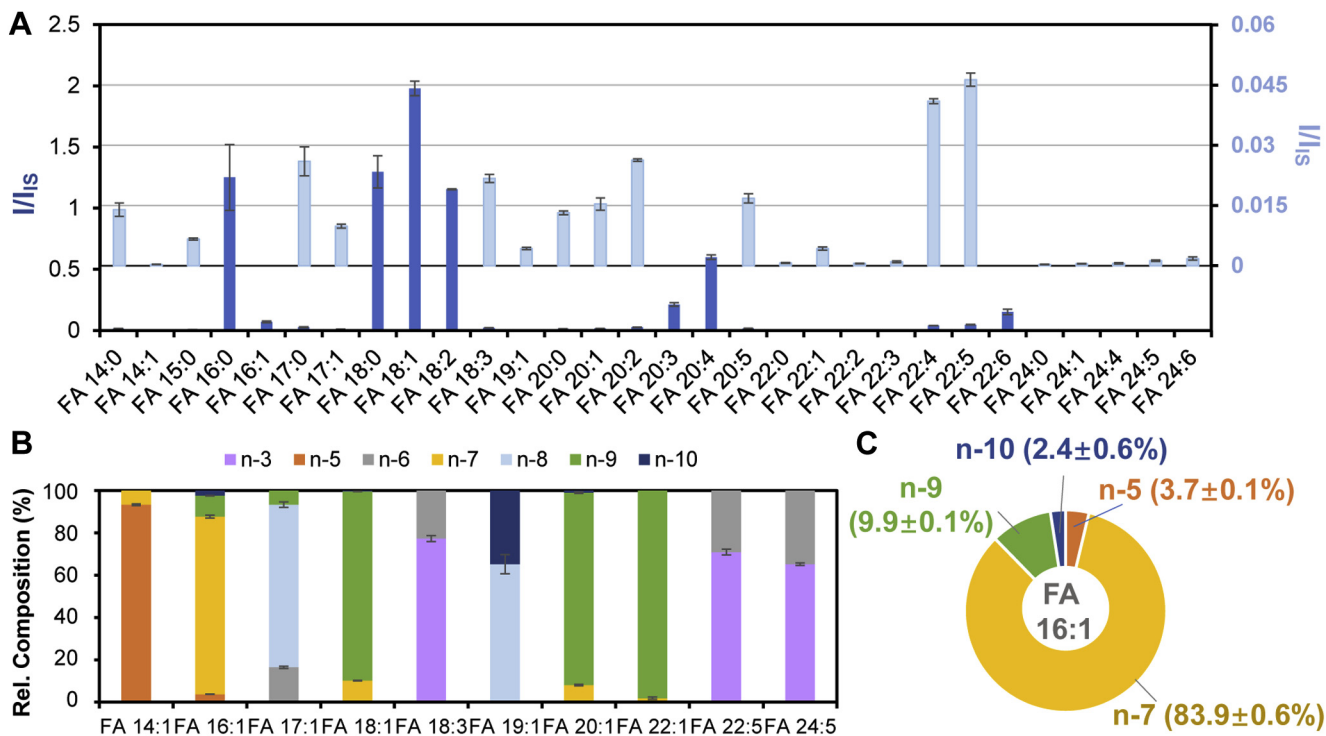
Fig. 6. A: Relative quantitation of total FAs at sum composition level in pooled human plasma. B: Relative composition (%) of C=C location isomers in eight groups of FAs. Error bars represent standard deviation of the mean (N = 3). C: Relative composition (%) of C=C location isomers of FA 16:1 in pooled human plasma.

isomer contributed $10.1 \pm 0.1\%$, and $0.5 \pm 0.1\%$, respectively. A full list of relative compositions of C=C location isomers is placed in supplemental Table S5.

The FFAs in pooled human plasma were analyzed following the same procedure. The summed concentration of FFAs was about one-tenth of the total FAs. Due to this reason, 23 FFAs were detected at sum composition level, less than the number detected for total FAs (30 species). However, the profile of FFAs was very similar to that of the total FAs, with FA 18:1 being the most abundant species, followed by FA 16:0 (supplemental Fig. S16). Twenty-eight unsaturated FFAs were identified at the C=C location level with relative isomer quantitation achieved for seven groups of isomers (supplemental Table S6). Several low-abundance isomers, which were detected from total FAs, such as FA 20:1 (n-10) and FA 22:5 (n-6), were not detected above noise level. The relative composition of C=C location isomers in each FA group, however, did not show big differences between FFA and total FA. For instance, the n-7 isomer contributed to $86.7 \pm 0.2\%$ and $83.9 \pm 0.6\%$ in the free form and esterified form of FA 16:1, respectively. The relative composition of the n-3 isomer of FA 18:3 was found higher in the free form ($88.7 \pm 0.1\%$) than that from the esterified one ($77\% \pm 1\%$). Compared with a previous GC-MS report (11), the established workflow shows an advantage of detecting minor isomers (~1% relative composition) such as FA 16:1(n-10) and FA 18:1(n-10) and PUFAs with very long chains (24 carbons).

Previous studies have attempted to link the change of both FFAs and total FAs with T2D diagnosis and therapy (49). The alteration of total FA profile at sum composition level was observed among hundreds of control, prediabetes, and diabetes sample (50). However, plasma lipids are often subjected to large concentration fluctuations due to diet and lifestyle (50), making it difficult for the discovery of plasma lipid markers. In previous studies, we found that the relative compositions of C=C location isomers were much less affected by interpersonal variations and the relative ratios of C18:1 n-9/n-7 isomers from several PC, PE, and PI molecules exhibited significant differences between control and T2D samples (29, 51). In this work, we compared the compositional changes of C=C location isomers of total FAs in human plasma between T2D patients (n = 6) and normal control (n = 6). From the MRM analysis, FA 16:0, FA 17:1, and FA 18:0 showed significant decreases in relative abundances in T2D relative to normal control (supplemental Fig. S17, two-tailed t test, $*P < 0.05$). This trend deviated from a large cohort study (50) and reflected that the profiles of plasma lipids were highly heterogeneous regarding to the samples used. Interestingly, although no significant change in relative abundances was found for FA 16:1 and FA 18:1 (Fig. 7A, B), the relative compositions of the n-10 isomers were significantly higher in T2D patients than that of normal control (two-tailed t test, $**P < 0.01$, $***P < 0.001$, Fig. 7C, D). Except for the n-10 isomers, there was no obvious trend in the relative
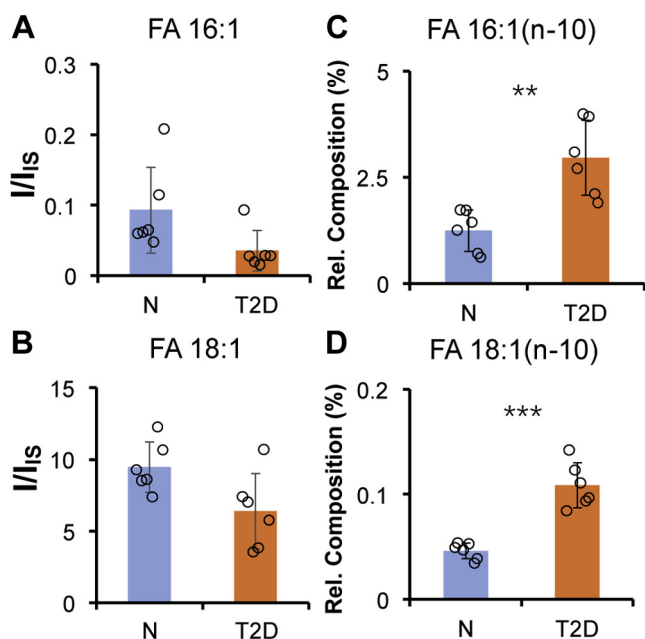
Fig. 7. Analysis of total FAs in human plasma samples, normal control (N, n = 6) versus T2D (n = 6). Relative quantitation of (A) FA 16:1 and (B) FA 18:1 at sum composition level. Relative composition (%) of n-10 C=C location isomers in (C) FA 16:1 and (D) FA 18:1. Statistical difference between the two groups was evaluated using the two-tailed student's *t* test (**$P < 0.01$, ***$P < 0.001$). Error bars represent standard deviation of the mean (n = 6).

compositional changes of the n-7 or n-9 isomers. As to PUFAs such as FA 18:3 and FA 22:5, the relative compositions of n-3 or n-6 isomer showed no significant change neither. Considering that the n-10 isomer is a characteristic metabolite of FADS2, further studies are needed to unravel the relationship between FADS2 activity and T2D.

DISCUSSION

In this work we have developed a sensitive workflow for global quantitation of FA at the double bond location level *via* an integration of two charge-derivatization steps, efficient RPLC separation, and structurally informative MS^2 CID. This workflow shows good tolerance to different matrixes, as demonstrated by deep structural annotation and relative quantitation of C=C location isomers from yak milk powder and human plasma. A total of 46 (32 unsaturated) FFAs from yak milk powder, 34 (28 unsaturated) FFAs, and 45 (37 unsaturated) total FAs from human plasma were identified. Relative quantitation of C=C location isomers was achieved for MUFAs (FA 14:1, 16:1, 17:1, 18:1, 19:1, 20:1, 22:1), PUFAs (FA18:3, 22:5, 24:5), and conjugated FAs (FA 18:2(n-7, n-9) and FA 18:2(n-6, n-8)). Profiling total FAs in plasma of T2D patients showed that the relative compositions of the n-10 isomers of FA 16:1 and FA 18:1 increased significantly relative to normal control. This information provides new insight into linking

FADS2 activity with T2D, which cannot be obtained without performing quantitation at C=C location level. Regarding the analytical performance, the developed method shows advantages in identifying unknown FAs where the synthetic standards are not available and detecting minor C=C location isomers as compared with GC-MS methods. Our method offers LOI in sub-nM or sub-pg range for synthetic standards, which is at least 10 times more sensitive than those reported from GC-MS (52), OzID (19), UVPD (53), or epoxidation followed by LC-MS/MS (54). This high sensitivity enables relative quantitation of low-abundance C=C location isomers, such as the n-5 (3.7 ± 0.1%) and n-10 (2.4 ± 0.6%) isomers of FA 16:1 besides the commonly reported n-7 (83.9 ± 0.6%) and n-9 (9.9 ± 0.1%) isomers in pooled human plasma. However, the developed method cannot differentiate methyl branched FAs from the straight-chain FAs as demonstrated by GC-MS (14) and UVPD (53). Although the use of two RPLC-MS/MS runs takes about 30 min analysis time for each sample, it significantly reduces chemical interferences, thus enabling confident identification and relative quantitation of FAs of low abundances. The dual-derivatization strategy should be readily adapted for shotgun lipid analysis workflow to further improve the speed of analysis. Overall, the developed FA analysis workflow may serve as a powerful tool for deep profiling of FAs in both fundamental and clinical studies.

Author contributions

Y. X. conceptualization; J. Z. and M. F. data curation; J. Z., M. F., and Y. X. investigation; Y. X. and J. Z. methodology; J. Z., M. F., and Y. X. writing–original draft; Y. X., J. Z., and M. F. writing–review and editing.

Conflict of interest

The authors declare that they have no conflicts of interest with the contents of this article.

Abbreviations

AMPP, N-(4-aminomethylphenyl)pyridium; C=C, carbon-carbon double bond; FA, fatty acid; MRM, multiple reaction monitoring; MS/MS, tandem mass spectrometry; PB,

REFERENCES

1. Nakamura, M. T., Yudell, B. E., and Loor, J. J. (2014) Regulation of energy metabolism by long-chain fatty acids. *Prog. Lipid Res.* **53**, 124–144

2. Harayama, T., and Riezman, H. (2018) Understanding the diversity of membrane lipid composition. *Nat. Rev. Mol. Cell Biol.* **19**, 281–296

3. Marakalala, M. J., Raju, R. M., Sharma, K., Zhang, Y. J., Eugenin, E. A., Prideaux, B., Daudelin, I. B., Chen, P-Y., Booty, M. G., Kim, J. H., Eum, S. Y., Via, L. E., Behar, S. M., Barry, C. E., Mann, M., *et al.* (2016) Inflammatory signaling in human tuberculosis granulomas is spatially organized. *Nat. Med.* **22**, 531–538

4. Piccolis, M., Bond, L. M., Kampmann, M., Pulimeno, P., Chitraju, C., Jayson, C. B. K., Vaites, L. P., Boland, S., Lai, Z. W., Gabriel, K. R., Elliott, S. D., Paulo, J. A., Harper, J. W., Weissman, J. S., Walther, T. C., *et al.* (2019) Probing the global cellular responses to lipotoxicity caused by saturated fatty acids. *Mol. Cell.* **74**, 32–44. e38

5. Bond, L. M., Miyazaki, M., O'Neill, L. M., Ding, F., and Ntambi, J. M. (2016) Chapter 6 - Fatty Acid Desaturation and Elongation in Mammals. In *Biochemistry of Lipids, Lipoproteins and Membranes*, 6th Ed., N. D. Ridgway and R. S. McLeod, editors. Elsevier, Boston, MA, 185–208

6. Madore, C., Leyrolle, Q., Morel, L., Rossitto, M., Greenhalgh, A. D., Delpech, J. C., Martinat, M., Bosch-Bouju, C., Bourel, J., Rani, B., Lacabanne, C., Thomazeau, A., Hopperton, K. E., Beccari, S., Sere, A., *et al.* (2020) Essential omega-3 fatty acids tune microglial phagocytosis of synaptic elements in the mouse developing brain. *Nat. Commun.* **11**, 6133

7. Savino, A. M., Fernandes, S. I., Olivares, O., Zemlyansky, A., Cousins, A., Markert, E. K., Barel, S., Geron, I, Frishman, L., Birger, Y., Eckert, C., Tumanov, S., MacKay, G., Kamphorst, J. J., Herzyk, P., *et al.* (2020) Metabolic adaptation of acute lymphoblastic leukemia to the central nervous system microenvironment depends on stearoyl-CoA desaturase. *Nat. Cancer.* **1**, 998–1009

8. Vriens, K., Christen, S., Parik, S., Broekaert, D., Yoshinaga, K., Talebi, A., Dehairs, J., Escalona-Noguero, C., Schmieder, R., Cornfield, T., Charlton, C., Romero-Pérez, L., Rossi, M., Rinaldi, G., Orth, M. F., *et al.* (2019) Evidence for an alternative fatty acid desaturation pathway increasing cancer plasticity. *Nature.* **566**, 403–406

9. Quehenberger, O., Armando, A. M., and Dennis, E. A. (2011) High sensitivity quantitative lipidomics analysis of fatty acids in biological samples by gas chromatography–mass spectrometry. *Biochim. Biophys. Acta.* **1811**, 648–656

10. Ecker, J., Scherer, M., Schmitz, G., and Liebisch, G. (2012) A rapid GC–MS method for quantification of positional and geometric isomers of fatty acid methyl esters. *J. Chromatogr. B.* **897**, 98–104

11. Chiu, H-H., and Kuo, C-H. (2020) Gas chromatography-mass spectrometry-based analytical strategies for fatty acid analysis in biological samples. *J. Food Drug Anal.* **28**, 60–73

12. Dobson, G., and Christie, W. W. (2002) Mass spectrometry of fatty acid derivatives. *Eur. J. Lipid Sci. Technol.* **104**, 36–43

13. Delmonte, P., and Rader, J. I. (2007) Evaluation of gas chromatographic methods for the determination of trans fat. *Anal. Bioanal. Chem.* **389**, 77–85

14. Wang, Z., Wang, D. H., Park, H. G., Tobias, H. J., Kothapalli, K. S. D., and Brenna, J. T. (2019) Structural identification of monounsaturated branched chain fatty acid methyl esters by combination of electron ionization and covalent adduct chemical ionization tandem mass spectrometry. *Anal. Chem.* **91**, 15147–15154

15. Van Pelt, C. K., and Brenna, J. T. (1999) Acetonitrile chemical ionization tandem mass spectrometry to locate double bonds in polyunsaturated fatty acid methyl esters. *Anal. Chem.* **71**, 1981–1989

16. Wang, M., Wang, C., Han, R. H., and Han, X. (2016) Novel advances in shotgun lipidomics for biology and medicine. *Prog. Lipid Res.* **61**, 83–108

17. Wang, M., Han, R. H., and Han, X. (2013) Fatty acidomics: global analysis of lipid species containing a carboxyl group with a charge-remote fragmentation-assisted approach. *Anal. Chem.* **85**, 9312–9320

18. Cheng, C., and Gross, M. L. (2000) Applications and mechanisms of charge-remote fragmentation. *Mass Spectrom. Rev.* **19**, 398–420

19. Poad, B. L. J., Marshall, D. L., Harazim, E., Gupta, R., Narreddula, V. R., Young, R. S. E., Duchoslav, E., Campbell, J. L., Broadbent, J. A., Cvačka, J., Mitchell, T. W., and Blanksby, S. J. (2019) Combining charge-switch derivatization with ozone-induced dissociation for fatty acid analysis. *J. Am. Soc. Mass. Spectrom.* **30**, 2135–2143

20. Fang, M., Rustam, Y., Palmieri, M., Sieber, O. M., and Reid, G. E. (2020) Evaluation of ultraviolet photodissociation tandem mass spectrometry for the structural assignment of unsaturated fatty acid double bond positional isomers. *Anal. Bioanal. Chem.* **412**, 2339–2351

21. Narreddula, V. R., McKinnon, B. I., Marlton, S. J. P., Marshall, D. L., Boase, N. R. B., Poad, B. L. J., Trevitt, A. J., Mitchell, T. W., and Blanksby, S. J. (2021) Next-generation derivatization reagents optimized for enhanced product ion formation in photodissociation-mass spectrometry of fatty acids. *Analyst.* **146**, 156–169

22. Randolph, C. E., Foreman, D. J., Betancourt, S. K., Blanksby, S. J., and McLuckey, S. A. (2018) Gas-phase ion/ion reactions involving tris-phenanthroline alkaline earth metal complexes as charge inversion reagents for the identification of fatty acids. *Anal. Chem.* **90**, 12861–12869

23. Zhao, Y., Zhao, H., Zhao, X., Jia, J., Ma, Q., Zhang, S., Zhang, X., Chiba, H., Hui, S-P., and Ma, X. (2017) Identification and quantitation of C=C location isomers of unsaturated fatty acids by epoxidation reaction and tandem mass spectrometry. *Anal. Chem.* **89**, 10270–10278

24. Kuo, T-H., Chung, H-H., Chang, H-Y., Lin, C-W., Wang, M-Y., Shen, T-L., and Hsu, C-C. (2019) Deep lipidomics and molecular imaging of unsaturated lipid isomers: a universal strategy initiated by mCPBA epoxidation. *Anal. Chem.* **91**, 11905–11915

25. Unsihuay, D., Su, P., Hu, H., Qiu, J., Kuang, S., Li, Y., Sun, X., Dey, S. K., and Laskin, J. (2021) Imaging and analysis of isomeric unsaturated lipids through online photochemical derivatization of carbon–carbon double bonds. *Angew. Chem. Int. Ed.* **60**, 7559–7563

26. Ma, X., and Xia, Y. (2014) Pinpointing double bonds in lipids by Paternò-Büchi reactions and mass spectrometry. *Angew. Chem. Int. Ed.* **53**, 2592–2596

27. Ma, X., Chong, L., Tian, R., Shi, R., Hu, T. Y., Ouyang, Z., and Xia, Y. (2016) Identification and quantitation of lipid C=C location isomers: a shotgun lipidomics approach enabled by photochemical reaction. *Proc. Natl. Acad. Sci. U. S. A.* **113**, 2573

28. Su, Y., Ma, X., Page, J., Shi, R., Xia, Y., and Ouyang, Z. (2019) Mapping lipid C=C location isomers in organ tissues by coupling photochemical derivatization and rapid extractive mass spectrometry. *Int. J. Mass Spectrom.* **445**, 116206

29. Zhang, W., Zhang, D., Chen, Q., Wu, J., Ouyang, Z., and Xia, Y. (2019) Online photochemical derivatization enables comprehensive mass spectrometric analysis of unsaturated phospholipid isomers. *Nat. Commun.* **10**, 79

30. Wäldchen, F., Mohr, F., Wagner, A. H., and Heiles, S. (2020) Multifunctional reactive MALDI matrix enabling high-lateral resolution dual polarity MS imaging and lipid C=C position-resolved MS2 imaging. *Anal. Chem.* **92**, 14130–14138

31. Feng, G., Hao, Y., Wu, L., and Chen, S. (2020) A visible-light activated [2 + 2] cycloaddition reaction enables pinpointing carbon–carbon double bonds in lipids. *Chem. Sci.* **11**, 7244–7251

32. Wäldchen, F., Becher, S., Esch, P., Kompauer, M., and Heiles, S. (2017) Selective phosphatidylcholine double bond fragmentation and localisation using Paternò–Büchi reactions and ultraviolet photodissociation. *Analyst.* **142**, 4744–4755

33. Murphy, R. C., Okuno, T., Johnson, C. A., and Barkley, R. M. (2017) Determination of double bond positions in polyunsaturated fatty acids using the photochemical Paternò-Büchi reaction with acetone and tandem mass spectrometry. *Anal. Chem.* **89**, 8545–8553

34. Ma, X., Zhao, X., Li, J., Zhang, W., Cheng, J-X., Ouyang, Z., and Xia, Y. (2016) Photochemical tagging for quantitation of

unsaturated fatty acids by mass spectrometry. *Anal. Chem.* **88**, 8931–8935

35. Xu, S.-l., Wu, B.-f., Orešič, M., Xie, Y., Yao, P., Wu, Z.-y., Lv, X., Chen, H., and Wei, F. (2020) Double derivatization strategy for high-sensitivity and high-coverage localization of double bonds in free fatty acids by mass spectrometry. *Anal. Chem.* **92**, 6446–6455

36. Esch, P., and Heiles, S. (2018) Charging and charge switching of unsaturated lipids and apolar compounds using Paternò-Büchi reactions. *J. Am. Soc. Mass. Spectrom.* **29**, 1971–1980

37. Xie, X., Zhao, J., Lin, M., Zhang, J-L., and Xia, Y. (2020) Profiling of cholesteryl esters by coupling charge-tagging Paternò–Büchi reaction and liquid chromatography–mass spectrometry. *Anal. Chem.* **92**, 8487–8496

38. Zhao, J., Xie, X., Lin, Q., Ma, X., Su, P., and Xia, Y. (2020) Next-generation Paternò–Büchi reagents for lipid analysis by mass spectrometry. *Anal. Chem.* **92**, 13470–13477

39. Dugave, C., and Demange, L. (2003) Cis−Trans Isomerization of Organic Molecules and Biomolecules: Implications and Applications. *Chem. Rev.* **103**, 2475–2532

40. Young, R. S. E., Bowman, A. P., Williams, E. D., Tousignant, K. D., Bidgood, C. L., Narreddula, V. R., Gupta, R., Marshall, D. L., Poad, B. L. J., Nelson, C. C., Ellis, S. R., Heeren, R. M. A., Sadowski, M. C., and Blanksby, S. J. (2021) Apocryphal FADS2 activity promotes fatty acid diversification in cancer. *Cell Rep.* **34**, 108738

41. Wallace, R. J., McKain, N., Shingfield, K. J., and Devillard, E. (2007) Isomers of conjugated linoleic acids are synthesized via different mechanisms in ruminal digesta and bacteria. *J. Lipid Res.* **48**, 2247–2254

42. Chilliard, Y., Glasser, F., Ferlay, A., Bernard, L., Rouel, J., and Doreau, M. (2007) Diet, rumen biohydrogenation and nutritional quality of cow and goat milk fat. *Eur. J. Lipid Sci. Technol.* **109**, 828–855

43. Xie, X., and Xia, Y. (2019) Analysis of conjugated fatty acid isomers by the Paternò-Büchi reaction and trapped ion mobility mass spectrometry. *Anal. Chem.* **91**, 7173–7180

44. Bollinger, J. G., Rohan, G., Sadilek, M., and Gelb, M. H. (2013) LC/ESI-MS/MS detection of FAs by charge reversal derivatization with more than four orders of magnitude improvement in sensitivity. *J. Lipid Res.* **54**, 3523–3530

45. Yu, E., and Hu, F. B. (2018) Dairy products, dairy fatty acids, and the prevention of cardiometabolic disease: a review of recent evidence. *Curr. Atheroscler. Rep.* **20**, 24

46. Liu, H. N., Ren, F. Z., Jiang, L., Ma, Z. L., Qiao, H. J., Zeng, S. S., Gan, B. Z., and Guo, H. Y. (2011) Short communication: Fatty acid profile of yak milk from the Qinghai-Tibetan Plateau in different seasons and for different parities. *J. Dairy Sci.* **94**, 1724–1731

47. Guijas, C., Meana, C., Astudillo, A. M., Balboa, M. A., and Balsinde, J. (2016) Foamy monocytes are enriched in cis-7-hexadecenoic fatty acid (16:1n-9), a possible biomarker for early detection of cardiovascular disease. *Cell Chem. Biol.* **23**, 689–699

48. Park, H. G., Kothapalli, K. S. D., Park, W. J., DeAllie, C., Liu, L., Liang, A., Lawrence, P., and Brenna, J. T. (2016) Palmitic acid (16:0) competes with omega-6 linoleic and omega-3 α-linolenic acids for FADS2 mediated Δ6-desaturation. *Biochim. Biophys. Acta.* **1861**, 91–97

49. Palomer, X., Pizarro-Delgado, J., Barroso, E., and Vázquez-Carrera, M. (2018) Palmitic and oleic acid: the yin and yang of fatty acids in type 2 diabetes mellitus. *Trends Endocrin. Met.* **29**, 178–190

50. Li, N., Qiu, Y., Wu, Y., Zhang, M., Lai, Z., Wang, Q., Du, Y., Guo, L., Liu, S., and Li, Z. (2020) Association of serum total fatty acids with type 2 diabetes. *Clin. Chim. Acta.* **500**, 59–68

51. Xia, T., Ren, H., Zhang, W., and Xia, Y. (2020) Lipidome-wide characterization of phosphatidylinositols and phosphatidylglycerols on C=C location level. *Anal. Chim. Acta.* **1128**, 107–115

52. Han, L-D, Xia, J-F, Liang, Q-L, Wang, Y., Wang, Y-M, Hu, P., Li, P., and Luo, G-A. (2011) Plasma esterified and non-esterified fatty acids metabolic profiling using gas chromatography–mass spectrometry and its application in the study of diabetic mellitus and diabetic nephropathy. *Anal. Chim. Acta.* **689**, 85–91

53. Narreddula, V. R., Boase, N. R., Ailuri, R., Marshall, D. L., Poad, B. L. J., Kelso, M. J., Trevitt, A. J., Mitchell, T. W., and Blanksby, S. J. (2019) Introduction of a fixed-charge, photolabile derivative for enhanced structural elucidation of fatty acids. *Anal. Chem.* **91**, 9901–9909

54. Feng, Y., Chen, B., Yu, Q., and Li, L. (2019) Identification of double bond position isomers in unsaturated lipids by m-CPBA epoxidation and mass spectrometry fragmentation. *Anal. Chem.* **91**, 1791–1795